Cover Picture: Studies of Glutathione Transferase P1-1 Bound to a Platinum(IV)-Based Anticancer Compound Reveal the Molecular Basis of Its Activation (Chem. Eur. J. 28/2011)

ARTICLE *in* CHEMISTRY - A EUROPEAN JOURNAL · JULY 2011

Impact Factor: 5.73 · DOI: 10.1002/chem.201100586 · Source: PubMed

CHEMISTRY
A EUROPEAN JOURNAL

DOI: 10.1002/chem.201100586

Studies of Glutathione Transferase P1-1 Bound to a Platinum(IV)-Based Anticancer Compound Reveal the Molecular Basis of Its Activation

Lorien J. Parker,[a, b] Louis C. Italiano,[a, b] Craig J. Morton,[a] Nancy C. Hancock,[a] David B. Ascher,[a] Jade B. Aitken,[c] Hugh H. Harris,[d] Pablo Campomanes,[e] Ursula Rothlisberger,[e] Anastasia De Luca,[f] Mario Lo Bello,[f] Wee Han Ang,[g] Paul J. Dyson,[e] and Michael W. Parker*[a, b]

Abstract: Platinum-based cancer drugs, such as cisplatin, are highly effective chemotherapeutic agents used extensively for the treatment of solid tumors. However, their effectiveness is limited by drug resistance, which, in some cancers, has been associated with an overexpression of pi class glutathione S-transferase (GST P1-1), an important enzyme in the mercapturic acid detoxification pathway. Ethacraplatin (EA-CPT), a *trans*-Pt^{IV} carboxylate complex containing ethacrynate ligands, was designed as a platinum cancer metallodrug that could also target cytosolic GST enzymes. We previously reported that EA-CPT was an excellent inhibitor of GST activity in live mammalian cells compared to either cisplatin or ethacrynic acid. In order to understand the nature of the drug–protein interactions between EA-CPT and GST P1-1, and to obtain mechanistic insights at a molecular level, structural and biochemical investigations were carried out, supported by molecular modeling analysis using quantum mechanical/molecular mechanical methods. The results suggest that EA-CPT preferentially docks at the dimer interface at GST P1-1 and subsequent interaction with the enzyme resulted in docking of the ethacrynate ligands at both active sites (in the H-sites), with the Pt moiety remaining bound at the dimer interface. The activation of the inhibitor by its target enzyme and covalent binding accounts for the strong and irreversible inhibition of enzymatic activity by the platinum complex.

Keywords: antitumor agents · detoxification · ethacrynic acid · glutathione transferases · X-ray crystallography

Introduction

Cisplatin (CPT) is an FDA-approved anticancer drug used widely in the treatment of solid tumors, including testicular, ovarian, cervical, bladder, head/neck and lung cancers.[1,2] Its mechanism of action occurs by a sequence of events including cell entry, activation, and DNA-binding. CPT binds nuclear DNA to form intra- or interstrand DNA cross-links that are effective inhibitors of replication and transcription processes.[3,4] In certain cancers, such as ovarian cancer, patients receiving CPT treatment develop resistance to the drug and require an increase in dosage levels to remain effective. One factor that has been implicated in the development of drug resistance is the overexpression of pi class glutathione S-transferase (GST P1-1).[5,6] GST P1-1 belongs to the class of GST detoxification enzymes (EC 2.5.1.18), the principal role of

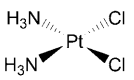

cisplatin

[a] L. J. Parker, L. C. Italiano, C. J. Morton, N. C. Hancock, D. B. Ascher, M. W. Parker
Biota Structural Biology Laboratory
St. Vincent's Institute of Medical Research
41 Victoria Parade, Fitzroy, Victoria 3065 (Australia)
Fax: (+61) 3-9416-2676
E-mail: mparker@svi.edu.au

[b] L. J. Parker, L. C. Italiano, M. W. Parker
Department of Biochemistry and Molecular Biology
Bio21 Molecular Science and Biotechnology Institute
The University of Melbourne, 30 Flemington Road
Parkville, Victoria 3010 (Australia)

[c] J. B. Aitken
School of Chemistry, The University of Sydney
New South Wales 2006 (Australia)

[d] H. H. Harris
School of Chemistry and Physics
University of Adelaide, South Australia 5005 (Australia)

[e] P. Campomanes, U. Rothlisberger, P. J. Dyson
Institut des Sciences et Ingénierie Chimiques
Ecole Polytechnique Fédérale de Lausanne (EPFL)
1015 Lausanne (Switzerland)

[f] A. De Luca, M. Lo Bello
Department of Biology, University of Rome Tor Vergata
Via della Ricerca Scientifica 1, Rome 00133 (Italy)

[g] W. H. Ang
Department of Chemistry
National University of Singapore
3 Science Drive 3, Singapore 117543 (Singapore)

Supporting information for this article is available on the WWW under http://dx.doi.org/10.1002/chem.201100586.

which is to catalyze the conjugation of xenobiotics to glutathione (GSH), the first step in the mercapturic acid pathway that leads to elimination of toxic compounds.

Human cytosolic GSTs are dimeric proteins that can be grouped into at least seven gene-independent classes (alpha, mu, pi, sigma, theta, omega, and zeta) on the basis of their amino acid sequence.[7,8] Their three-dimensional folds do not differ significantly despite low sequence homologies. Each subunit contains a very similar binding site for GSH (G-site) and a second binding site for the hydrophobic co-substrate (H-site) with structural differences in the latter conferring some substrate selectivity.[7–9] Several GST isoforms have been strongly associated with various malignancies, particularly in the development of drug resistance towards certain widely used chemotherapies. For example, marked overexpression of GST P1-1 has been observed following the exposure of several tumor cell lines to various tumor drugs[5] and hence the enzyme is used as a biomarker. GST P1-1 is also overexpressed in CPT-resistant cell lines[10,11] and the inhibition of the enzyme has been shown to reverse resistance.[6] In addition, GST P1-1 knockout mice are considerably more sensitive to the cytotoxic effects of CPT treatment than their wild-type counterparts.[12]

The development of small molecules capable of effectively inhibiting GST activity is a subject of intense research interest. Ethacrynic acid (EA) is a diuretic in clinical use and a potent inhibitor of GST that has been extensively investi-

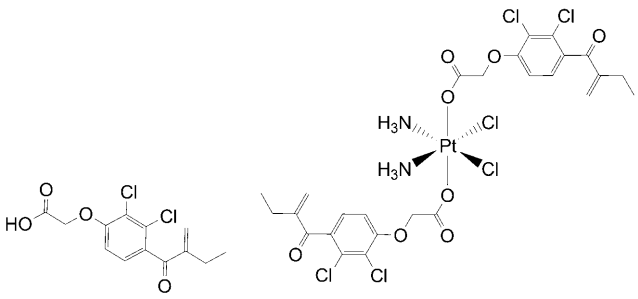

gated.[13,14] Clinical trials using EA as an adjuvant with either chlorambucil, thiotepa, or CPT met with limited success, presumably due to the differential uptake of the administered drugs.[15] In order to optimize this delivery strategy, we conceived a platinum-based small-molecule complex to target cytosolic GST enzymes in addition to DNA, which is the conventional target of platinum-based chemotherapeutics. The metallocomplex comprises a *trans*-platinum(IV) carboxylate complex containing GST inhibitors as ligands that are released upon reduction.[16] The target molecule, ethacraplatin (EA-CPT), contains two EA moieties on the axial positions of a *cis,cis,trans*-diamminedichloridobiscarboxylatoplatinum(IV) framework with a CPT moiety at the equatorial site. After cell entry, the compound can be reduced intracellularly to release a cytotoxic Pt^{II} moiety as well as two EA moieties capable of inhibiting GST enzymes. In an earlier report, we observed strong inhibition of GST activity by EA-CPT against recombinant GST P1-1 and GST A1-1 enzymes, at levels tenfold higher than EA.[16] It was also found that the GST activity of cellular extracts of treated A549 cells were low, indicating that EA-CPT was able to penetrate live mammalian cells and inhibit their GST activity. In addition, EA-CPT inhibited the cell viability of a panel of carcinoma cell lines at levels comparable to CPT.

To understand the nature of the drug–protein interaction, we have conducted biochemical studies using EA-CPT with recombinant GST P1-1, the most abundant GST isoform in cancer cells. Structural analysis into the binding of EA-CPT to GST P1-1 has been carried out using single-crystal X-ray crystallographic methods and X-ray absorption spectroscopy (XAS). Finally, molecular modeling based on quantum mechanical/molecular mechanical (QM/MM) simulations was undertaken to provide insights into the mechanism of binding between the platinum complex and its protein target.

Results

Enzyme inhibition studies of GST P1-1 wild-type with EA-CPT: When GST P1-1 was incubated with different amounts of EA-CPT, we observed a stronger inhibitory effect of this new compound in comparison with EA alone or in combination with CPT (Figure 1). CPT did not inhibit GST activity on its own. The IC_{50} values, reported in Table 1, showed a 20-fold increase in the inhibitory potency of EA-CPT (0.54 μM) in comparison with EA. In contrast, an IC_{50} was not detectable for CPT, due to its poor inhibitory activity towards GST P1-1, demonstrating the importance of the EA moiety of EA-CPT for inhibition. EA-CPT behaved like EA in that it was also a non-competitive inhibitor towards GSH and a competitive inhibitor towards 1-chloro-2,4-dinitrobenzene (CDNB; Figure 1). We derived the values of K_i^{GSH} of 0.17 ± 0.05 μM, and K_i^{CDNB} of 0.14 ± 0.02 μM for EA-CPT from double reciprocal plots (Table 2). These new values were significantly lower than those obtained for EA alone, indicating that the mode of inhibition by EA-CPT may be similar to EA but with a greater potency.

Crystallographic studies: The model of GST P1-1 complexed to EA-CPT has been refined to a resolution of 1.85 Å (Table 3). One major peak of 8σ was observed in the F_o-F_c difference electron map, located at the dimer interface and was interpreted as a Pt ion bound to one Cys101 S-atom from each monomer (Figure 2a) with an average Pt–S distance of 2.4 Å, a typical value for such bonds. An anomalous difference Fourier map, calculated from the same data collected at a wavelength of 1.54 Å, showed a peak of 8.5σ in the same position, thus confirming the identity of the peak as a Pt ion. The Pt ion was refined to an occupancy of 0.2 with a *B*-factor of 30 $Å^2$, the same value as protein-bound water molecules nearby. The Pt is bound in a *trans* geome-

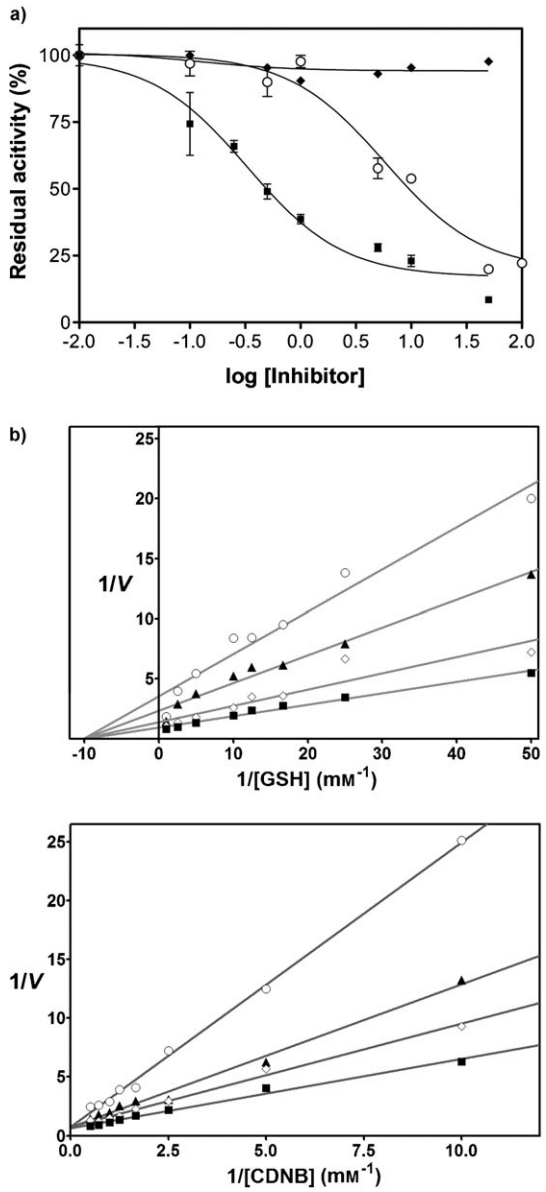

Figure 1. Kinetic studies of GST P1-1 binding to EA-CPT. a) Determination of the inhibitory effect of CPT (◆), EA (○) and EA-CPT (■) on GST P1-1. b) Double reciprocal plots for the CDNB/GSH conjugation by GST P1-1 in presence of increasing concentrations of EA-CPT. Assay conditions and data analysis are reported in the Experimental Section. Shown are plots of GSH (top panel) and CDNB (bottom panel), as the variable substrate, in the presence of different, fixed EA-CPT concentrations (0 (■), 0.1 (◇), 0.3 (▲), 0.5 μM (○)). From this set of reciprocal plots the K_i^{GSH} and K_i^{CDNB} values were obtained.

Table 1. IC_{50} values for CPT, EA and EA-CPT binding to GST P1-1.

Compound	IC_{50} [μM]
CPT	–
EA	10.9 ± 1.14
EA-CPT	0.54 ± 0.12

try, consistent with a reduction of Pt^{IV} to Pt^{II} with a concomitant reduction in the coordination number from six to four.

Table 2. Inhibition rate constant, K_i [μM], for EA and EA-CPT binding to GST P1-1.

Compound	K_i^{GSH}	K_i^{CDNB}
EA	22.4 ± 1.83	11.4 ± 1.45
EA-CPT	0.17 ± 0.05	0.14 ± 0.02

There was no extra density to suggest the EA moiety was still attached to the Pt ion. There was a small amount of density for one Pt ligand, in addition to two Cys101, which we interpreted as a chloride ligand based on the high concentration of chloride ions in the crystallization medium. In addition, electron density for an EA molecule was evident in the active site of each subunit (Figure 2b). The density for the arene ring and its chloride atoms was clearly defined, whereas density for the butryl moiety was mostly missing. There were also anomalous peaks, measuring 4σ, at the positions that correspond to the chloride atoms for each of the EA moieties (Figure 2b). EA was built into the model and refined to 50% occupancy with an average *B*-factor of 27.6 Å^2, which is similar to the surrounding residues (18–26 Å^2). The EA molecule sits in a hydrophobic pocket lined with the side-chains of Tyr7, Phe8, Pro9, and Val10 and the aliphatic portions of Arg13, Val35, Ile104, Tyr108, as well as Gly205. Its ring stacks between the aromatic side-chains of Phe8 and Tyr108. The two chloride groups are nestled in a pocket formed by Tyr7, Phe8, Val10, Tyr108, and Gly205 (Figure 2c). The carboxylate has interactions with the nitrogen atoms in the side-chain of Arg13 as well as the hydroxyl group of Tyr7. It also has water-mediated interactions with Tyr7, Leu52, Tyr108, and Asn204 and van der Waals interactions with the backbone of Gly12 and Arg13 as well as the side-chain of Ile104. The butryl moiety points towards the solvent, and consequently does not interact with the protein (Figures 2 and 3). Superposition of the EA-CPT complex onto the previously determined EA complex (PDB id: 2GSS)[17] shows the protein structures are essentially identical with a root-mean-square deviation in α-carbon positions of 0.2 Å for 416 residues and the EA ligands bind the same way (Figure 2c). There are no significant movements of side-chains in the active site or at the dimer interface with the exception of Cys101 that adopts two conformations, the usual one and another rotamer in which the thiol side-chain has rotated to interact with the Pt ion in the dimer interface.

QM/MM molecular dynamics simulations of EA-CPT binding at the dimer interface: To establish the nature of some exogenous ligands coordinated to the Pt center, which could not be discerned from the electron density map in the final crystal structure, we aimed to identify the most plausible Pt coordination environment by means of QM/MM MD simulations. To this end, the reactive part of the system, namely the Pt ion and the ligands directly coordinated to it, including both Cys101 side chains up to the β-carbon atom, was treated at the density functional theory (DFT) level, whereas the remaining part of the system, including water molecules and counterions, was modeled at a classical level. Sev-

Table 3. Summary of data collection and refinement of the EA-CPT GST P1-1 complex.

Data collection	
T [K]	100
space group	$C2$
cell dimensions	
a [Å]	76.8
b [Å]	90.0
c [Å]	68.9
β [°]	98.2
maximum resolution [Å]	1.85
no. crystals	1
no. observations	144159
no. unique reflections	39484
data completeness [%]	99.8 (99.8)[a]
R_{merge}[b]	6.3 (40.0)
I/σ_I	10.4 (1.9)
multiplicity	3.7
Refinement	
non-hydrogen atoms	
protein	3302
Pt	1
EA	38
GSH	0
MES	24
Ca^{2+}	3
Cl^-	1
solvent (H_2O)	379
resolution [Å]	1.85
R_{cryst}[c] [%]	17.6
R_{free}[d] [%]	21.5
reflections used in R factor calculations	37457
rmsd's from ideal geometry	
bonds [Å]	0.018
angles [°]	1.6
mean B (protein) [Å^2]:	
main-chain	19.2
side-chain	20.6
mean B (solvent) [Å^2]	27.1
mean B (Pt) [Å^2]	30.0
mean B (EA) [Å^2]	27.6
residues in most favored regions of Ramachandran plot [%]	92.7
residues in disallowed regions of Ramachandran plot [%]	0

[a] The values in parentheses are for the highest resolution bin. [b] $R_{merge}=\Sigma_{hkl}\Sigma_i|I_i-\langle I\rangle|/|\langle I\rangle|$, where I_i is the intensity for the ith measurement of an equivalent reflection with indices h,k,l. [c] $R_{cryst}=\Sigma||F_o|-|F_c||/\Sigma|F_o|$, in which F_o and F_c are the observed and calculated structure factor amplitudes, respectively. [d] R_{free} was calculated with 5% of the diffraction data that were selected randomly and not used throughout refinement.

eral models differing in the ligands directly coordinated to the Pt were taken into consideration (Figure 4) and their geometrical features were compared with those appearing in the crystal structure of the GST P1-1 EA-CPT complex. These results, displayed in Table 4, show that a fourth ligand is required to stabilize the Pt compound. In the absence of some exogenous ligand *trans* to the Cl ligand, the geometry of the S-Pt-S angle, in particular, was clearly distorted after only a few ps of simulation. However, when either a neutral (ammine or water) or an anionic moiety (hydroxyl or chloride) is included as an additional ligand in the simulations, all the angles and distances involving the Pt center are consistent with the experimental values.

To investigate the effects caused by the presence of these exogenous ligands in their nearest protein environment, a local root-mean-square deviation (RMSD) encompassing all the residues that are in the second coordination sphere around the metal center was defined, thus permitting the deviations from the crystal structure to be quantified (Table 4). The closest match with the crystal structure was obtained when a hydroxyl group (OH) was incorporated as a fourth ligand in the simulations. However, taking into account the small differences in the RMSD values obtained and the resolution of the crystal structure, the possibility of having either water or ammine ligand occupying the vacant position in the coordination sphere around the Pt center cannot be ruled out. In contrast, a high RMSD found when a second Cl ligand was bound to the Pt precluded the possibility of finding this coordination environment around the metal center. This high RMSD is mainly due to the spatial reorientation suffered by the side-chains of the residues that are next to the Cl ligand as a consequence of the presence of a second Cl substituent coordinated to the metal center.

X-ray absorption near edge structure (XANES) studies: Pt L_3-edge XANES data were collected from a 1 mM GST P1-1 sample that had been incubated for 10 h with a sevenfold excess of EA-CPT and subsequently dialyzed to remove any excess EA-CPT. Figure 5 shows the background-subtracted and normalized edge spectrum, which is identical to that of Pt^{II} model compounds published previously[18] in terms of edge energy and, more importantly, the peak-height-to-edge jump intensity ratio, determined here to be 1.47, is consistent with the published value of 1.52. This indicates that EA-CPT was reduced by reaction with GST P1-1 in the absence of GSH, regardless of where it eventually binds to the dimer in solution.

Molecular dynamics simulations of the recognition mechanism of EA-CPT by GST P1-1: To investigate where the initial binding between EA-CPT and GST P1-1 takes place, the free-energy profile corresponding to both the approach of EA-CPT to the binding site at the dimer interface (between the two Cys101) and its docking into the H-site of one of the monomers through one of the EA ligands was estimated by using the metadynamics algorithm within the framework of classical MD simulations.[19,20] This technique has been shown to be a useful and accurate method in docking simulations, allowing different binding poses to be efficiently explored and their associated free-energy profiles constructed.[21,22]

The initial configuration and the collective variables (CVs) used to study the approach of EA-CPT to the Cys101 residues at the dimer interface are displayed in Figure 6a, and the free-energy landscape reconstructed as a function of those CVs is shown in Figure S1a in the Supporting Information. Two minima (M1 and M2) were sampled during the metadynamics simulations. The results indicate that the ap-

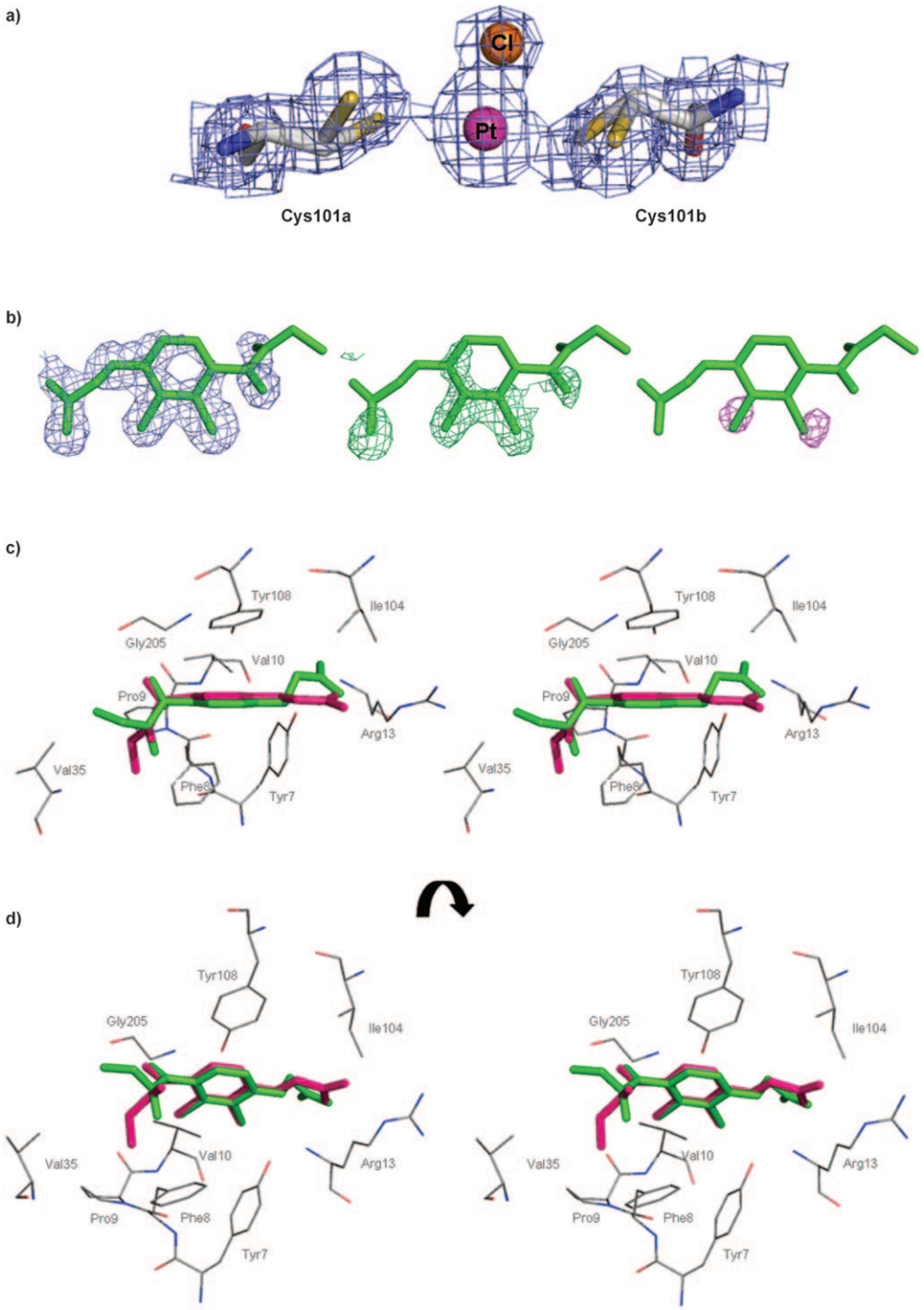

Figure 2. EA-CPT binding to GST P1-1. a) Binding to the dimer interface of wild-type enzyme. The final $2F_o-F_c$ electron density map in blue (contour level 1σ). Cys101 adopts two distinct conformations. The Pt ion is represented by a purple sphere and the chloride ligand is represented by an orange sphere. b) Binding to the active site of wild-type enzyme. The $2F_o-F_c$ density is shown in blue mesh and contoured at 1σ. The F_o-F_c electron density calculated after omitting EA from the model is shown in green mesh at 3σ. Anomalous peaks for the chloride atoms are shown in pink mesh contoured at 3σ. c) and d) Stereo superposition of the EA moiety of the wild-type EA-CPT structure onto the EA-wild-type GST complex structure (PDB id: 2GSS).[17] The surrounding side-chains are shown as lines and the EA moieties are shown as thick sticks (green for the structure presented here and pink for 2GSS).

proach of EA-CPT to a distance of about 7.5 Å from the binding site between both Cys residues is a barrierless process. At this configuration (M2), EA-CPT presents hydrophobic interactions with the side-chain of Thr109 of one of the monomers (A) and Val35 of the other (B) (Figure 6b). However, the entrance to the channel between both monomers is blocked by the presence of Tyr108 of monomer A and Thr109 of monomer B, which are in close proximity

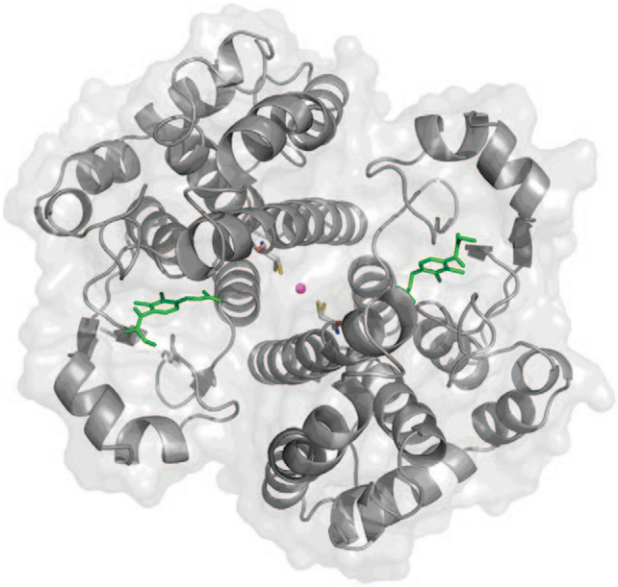

Figure 3. Surface and ribbon representations of EA-CPT binding to GST P1-1. The pink sphere is the Pt ion and the EA ligands are shown as green sticks. Both conformations of Cys101 are shown in grey sticks at the dimer interface.

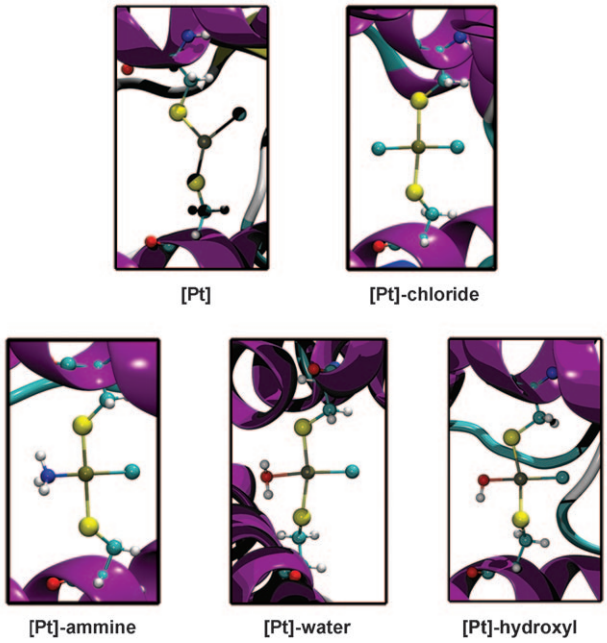

Figure 4. Models of Pt binding at the dimer interface taken into consideration in the QM/MM MD simulations. The protein is shown as purple ribbon and atoms shown with standard coloring.

(6.8 Å). These two residues must move apart to permit EA-CPT to move closer to both Cys101 residues. At M1, 2.5 kcal mol^{-1} lower in energy than M2, one of the EA moieties is involved in a π–π stacking interaction with a Tyr108 of monomer B, thus contributing to a further stabilization of this configuration (Figure 6c). The free-energy barrier associated with the evolution of the system from M2 to M1 is 7.6 kcal mol^{-1}.

Table 4. Mean values of selected geometrical parameters and root-mean-square deviations (RMSD) from the crystal structure for the different QM/MM MD simulations performed. Standard deviations are given in parentheses.

	Pt–Cl [Å]	Pt–S [Å]	S-Pt-S [°]	RMSD [Å]
X-ray structure	2.33	2.50	168.1	–
[Pt][a]	2.35 (0.04)	2.30 (0.06)	131.6 (7.9)	1.38 (0.03)
[Pt]–ammine	2.39 (0.06)	2.42 (0.06)	166.9 (3.7)	0.96 (0.04)
[Pt]–water	2.34 (0.04)	2.41 (0.06)	165.0 (4.5)	1.18 (0.05)
[Pt]–hydroxyl	2.46 (0.07)	2.42 (0.06)	168.6 (4.2)	0.68 (0.05)
[Pt]–chloride	2.41 (0.06)	2.43 (0.05)	172.3 (5.8)	3.57 (0.18)

[a] [Pt] refers to [Pt(Cys)$_2$Cl] core unit that was determined from the solid-state crystal structure.

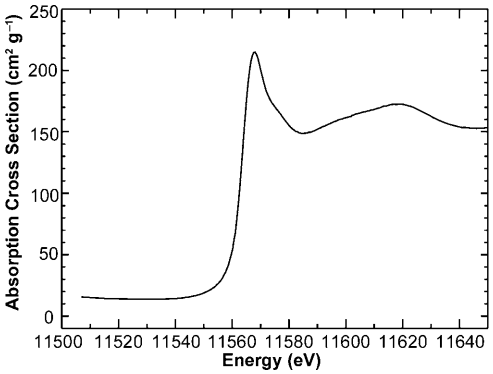

Figure 5. Pt L_3-edge frozen solution XANES spectrum of the EA-CPT/GST P1-1 reaction mixture.

The CVs employed to investigate the docking of EA-CPT into the H-site of one of the monomers are shown in Figure 7a, and the free-energy landscape corresponding to this process is displayed in Figure S1b in the Supporting Information. As in the case discussed above, two minima were sampled during our simulations. At M2 (Figure 7b), EA-CPT is H-bonded to the OH group of Tyr108 of one of the monomers and exhibits hydrophobic interactions with Ala112 of the other. Remarkably, two key residues (Trp38 and Tyr108) play an important role acting as a gate and guarding the entrance of EA-CPT into the H-site (Figure 7b). These two residues must rotate and increase their mutual separation to allow the docking of EA-CPT into the H-site through one of its EA moieties (Figure 7c). At M1, which is 4.6 kcal mol^{-1} more stable than M2, several interactions between the EA fragment and the residues forming the H-site of the enzyme maintain the stability of this configuration. In particular, close contacts with Phe8, Pro9 and Gly205 side chains could be identified. The free-energy barrier corresponding to the evolution from M2 to M1 is 12.7 kcal mol^{-1}. Therefore, the calculations indicate that the initial approach of EA-CPT to the Pt binding site at the dimer interface is favored over docking into the H-site of the enzyme through one of the EA moieties by 5.1 kcal mol^{-1}. Moreover, it is noteworthy that the orienta-

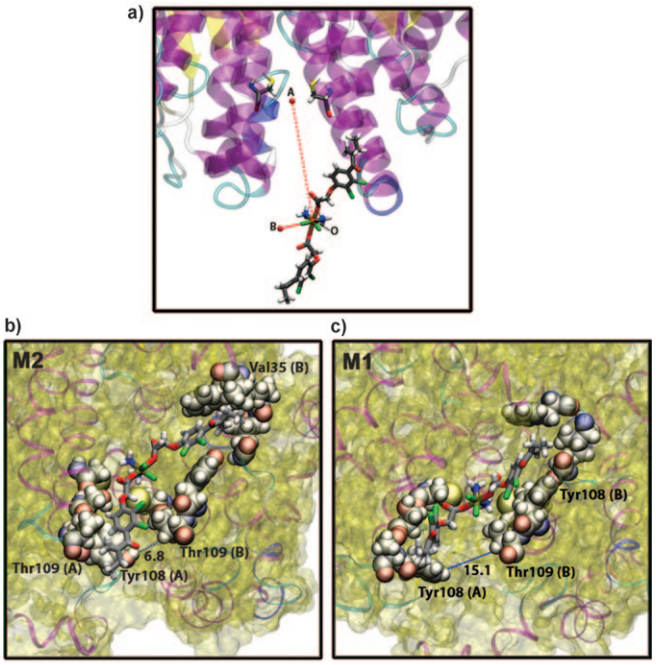

Figure 6. Metadynamics simulations of EA-CPT docking at the dimer interface. a) Collective variables (CV1 and CV2) employed to investigate the EA-CPT approach to the Cys101 residues at the dimer interface: CV1 is the distance OA between the Pt and the center of mass of both Cys101 residues, and CV2 is the angle AOB between the aforementioned points and one of the Cl atoms of EA-CPT. b) and c) Minimum free-energy configurations (M2 and M1, respectively) sampled during the simulations. Licorice and VdW representations respectively are used to visualize EA-CPT and some selected protein residues of both monomers (A or B).

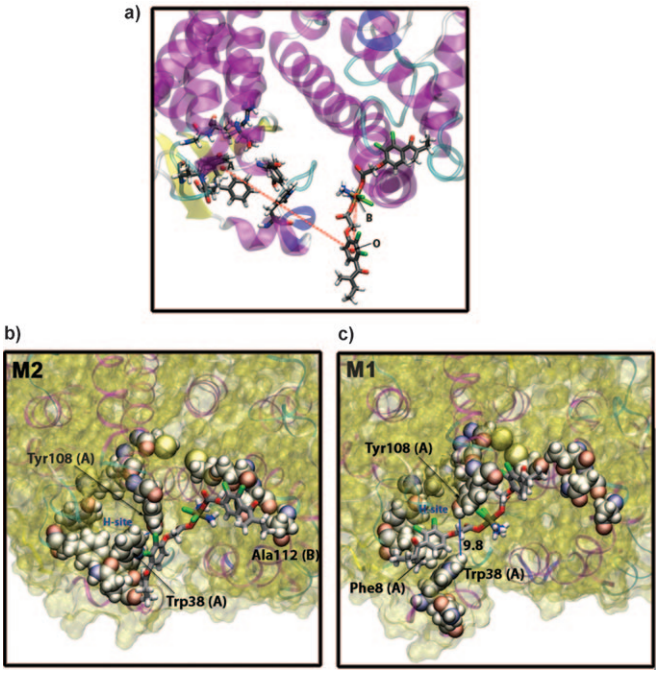

Figure 7. Metadynamics simulations of EA-CPT docking into one of the GST H-sites. a) Collective variables (CV1 and CV2) employed to investigate the docking event: CV1 is the distance OA between the centroid of the aromatic ring of one of the EA substituents and the center of mass of the protein residues that define the H-site of the protein, and CV2 is the angle AOB between the aforementioned points and the Pt. b) and c) Minimum free-energy configurations (M2 and M1, respectively) sampled during the simulations. Licorice and VdW representations respectively are used to visualize EA-CPT and some selected protein residues of both monomers (A or B).

tion that the EA ligands can adopt, once the drug is accommodated at the dimer interface (Figure S2 in the Supporting Information) and the corresponding Pt–O bond cleaved, would readily allow the diffusion of both fragments through the cavity between both monomers towards the H-site of the enzyme.

Discussion

This investigation demonstrates that EA-CPT is a more potent inhibitor of GST P1-1 than EA alone. Previously, we have observed, using ESI-MS, that incubation of wild-type GST P1-1 with EA-CPT for 2 h resulted in the formation of multiple adducts, which included the enzyme with EA, EA-CPT as well as both EA and Pt alone.[23] The presence of EA adducts suggests a role for GST P1-1 in reducing EA-CPT, presumably through the concomitant release of the Pt ion. This prompted us to carry out structural studies into the binding of wild-type GST P1-1 with EA-CPT by single-crystal X-ray diffraction. The resultant structure showed that wild-type GST P1-1 could reduce EA-CPT and bind both the Pt complex at the dimer interface and the released EA moieties at both H-sites. This provides a molecular-level explanation for the increased potency of EA-CPT as a GST inhibitor, which is able to covalently bind the Pt complex at the interface in addition to the EA substrates at the H-sites, as compared to EA.

A study on how EA-CPT binds at the dimer interface was carried out to provide details on the coordination sphere of the bound Pt center. EA-CPT fragments into several components when it binds to GST P1-1 (Figure 3). X-ray absorption near edge structure (XANES) analysis indicated that the bound metal is a Pt^{II} species and hence EA-CPT was reduced from Pt^{IV} after binding to the protein (Figures 2 and 5). The Pt moiety of EA-CPT binds at the dimer interface, utilizing the Cys101 S atom of each subunit as ligands in a *trans* arrangement. This is a plausible arrangement, because upon initial substitution of the first chloride ligand by a Cys101 S atom, the Pt–ammine bond *trans* to the new S ligand weakens, due to the strong *trans*-effect exerted by the S atom, allowing for substitution of the ammine by the Cys101 S atom from the second subunit, which is optimally situated. There was sufficient electron density from the X-ray crystallographic data to indicate that one of the remaining coordination sites was a chloride ligand. However, identification of the fourth ligand was not possible owing to insufficient electron density. Molecular dynamics simulations suggest that a hydroxyl, water or ammine ligand *trans* to the remaining chloride ligand (Figure 2) is most consistent with

the observed geometry (Figure 4), and it is unlikely that the Pt center maintained a vacant coordination site or has an additional chloride ligand.

Molecular modeling studies were undertaken to provide further insights into the manner in which EA-CPT first binds to GST P1-1. Two possibilities were considered: 1) through one of the EA ligands in the active site or 2) through the Pt center at the dimer interface, each of which imply a different mode of complex activation. In the first scenario it was assumed that the EA ligand would bind in a similar mode to previously reported GST P1-1+EA systems.[17,24] In one of these modes EA was stacked between the aromatic rings of Phe8 and Tyr108 with the carboxyl group directed towards the dimer interface (PDB id: 2GSS),[17] whereas in the other two modes the EA was conjugated to GSH, still stacked between the aromatic rings, but with the butryl moiety directed towards the dimer interface (PDB id: 3GSS, 11GS).[17,24] It should be noted that in both normal and cancer cells, GSH is expected to occupy the G-site, so GST P1-1 would catalyze the Michael addition of GSH to free EA. Attempts to model EA-CPT by superimposing one of its EA moieties onto EA-bound GST were straightforward: EA-CPT may bind in the H-site through one EA moiety with the rest of the compound pointing out to solution. However, it is not clear how the Pt center would be reduced and the EA moieties cleaved off in this binding mode. In the second scenario, EA-CPT was modeled into the dimer interface of GST P1-1. It is intriguing that the site could accommodate EA-CPT in a manner that both EA moieties of the complex are orientated in the same way as observed for the EA ligands in the active site of the GST P1-1+EA complex that was previously published (PDB id: 2GSS).[17]

This observation indicates that after reduction, the released EA ligands could diffuse through the water-filled cavity that extends from the dimer interface to the H-site, which only requires the EA ligand to transverse a short distance of 3 to 4 Å. Since the complex is symmetrically displaced about the twofold axis of the GST P1-1 dimer, this model would be consistent with the observation that both H-sites are occupied by EA ligands oriented in the same manner, consistent also with the crystal structure. It may therefore be postulated that EA-CPT first binds GST P1-1 at the dimer interface, where it is subsequently reduced and cleaved, permitting the diffusion of the EA fragments to both H-sites in the enzyme. As mentioned above, release of the Pt ion has been demonstrated directly by ESI-MS on the isolated enzyme; moreover, since EA-CPT is considerably more cytotoxic than EA on a series of cell lines,[16] it is not unreasonable to infer that this process also takes place in vivo.

Experimental Section

Materials: All chemical reagents were obtained from Sigma–Aldrich unless otherwise stated. EA-CPT was synthesized as described previously. Wild-type GST P1-1 was expressed and purified as previously described.[25] The protein was dialyzed overnight against buffer (10 mM phosphate pH 6.5, 0.1 mM ethylene diammine tetraacetic acid (EDTA), 0.1 mM dithiothreitol (DTT)) and then concentrated to 5–7 mg mL^{-1} using an Amicon Ultra-4 filter (MWCO 10,000) for crystallization. Purity was confirmed by SDS-PAGE.

Inhibition of GST P1-1 activity by EA, CPT and EA-CPT: Varying concentrations of EA, CPT, and EA-CPT (0.1–200 μM), pre-dissolved in DMSO or in ethanol (10 mM), were added to reaction mixtures of 1 mL final volume containing 1 mM GSH in buffer (100 mM potassium phosphate pH 6.5, 44 nM GST P1-1). The residual activity of GST P1-1 was assayed spectrophotometrically at 340 nm ($\varepsilon = 9600\,M^{-1}cm^{-1}$) upon the addition of the substrate, 1-chloro-2,4-dinitrobenzene (CDNB, final concentration 1 mM), at 25 °C. The IC_{50} for the inhibition of GST activity was determined by fitting the plot of residual GST activity against the inhibitor concentrations with a sigmoidal dose-response function using Prism (GraphPad).

The apparent K_m and V_{max} values of GST P1-1 were determined in the presence of EA and EA-CPT. Kinetic data were collected by varying GSH at a fixed CDNB concentration (and vice versa) with a fixed inhibitor concentration (2–50 μM for EA, 0.1–0.5 μM for EA-CPT). Apparent K_m and V_{max} values were obtained from Lineweaver–Burk plots using the program Prism (GraphPad). The K_i^{GSH} and K_i^{CDNB} values were derived from the different set of reciprocal plots.

Protein crystallization: Crystallization was performed by the hanging drop vapor diffusion method as previously described.[26] Briefly, a 2 μL drop of a protein solution (7 mg mL^{-1}; 10 mM phosphate pH 7.0, 1 mM EDTA and 1 mM mercaptoethanol) was mixed with an equivolume of reservoir buffer containing MES buffer (100 mM, pH 5.5 or 6.0), PEG 8000 (28% (w/v)), $CaCl_2$ (20 mM), and DTT (10 mM). All experiments were performed in the absence of GSH to prevent glutathionylation of the EA or reduction of EA-CPT. Crystals grew at 22 °C and reached a suitable size in approximately a week. A stock solution of EA-CPT was made up to 30 mM in DMSO and diluted 10 times in well solution containing MES (100 mM, pH 6.0), $CaCl_2$ (20 mM), and PEG 8000 (28% (w/v)). The final concentration of EA-CPT in the drop was approximately 3 mM. These crystals were frozen at half hour intervals after incubation in EA-CPT solution by soaking for two minutes in the reservoir solution plus 5% v/v methyl-2,4-pentanediol (MPD), then dipped briefly into a reservoir solution plus 10% v/v MPD. The crystals were then snap-frozen at 100 K in a cryostream. Soaks with higher EA-CPT concentrations and longer incubation times were also conducted but crystal quality deterioration was observed in all these experiments.

X-ray data collection and refinement: Diffraction data from a GST P1-1 frozen crystal, grown in the absence of GSH and soaked for 1.5 h in 3 mM EA-CPT, were collected in-house on an R-AXIS IV++ area detector with $Cu_{K\alpha}$ X-rays generated by a Rigaku MicroMax-007H rotating anode X-ray generator. The diffraction data were processed with the program MOSFLM[27] and scaled with SCALA.[28] An alternate round of scaling was performed with the anomalous flag on for the calculation of an anomalous difference Fourier map to identify the location of the Pt ions in the structure. Refinement began with the 5GSS model of GST P1-1 after GSH and water molecules were removed.[29] A round of rigid body refinement in REFMAC[30] was performed yielding an R_{cryst} of 30.8% (R_{free} of 31.7%). Water and MES were added using COOT,[31] interspersed by rounds of positional and isotropically restrained *B*-factor refinement using REFMAC.[30] After several rounds of refinement, electron density appeared in the H-site of both subunits consistent with EA molecules. EA was built into the $2F_o-F_c$ electron density map and refined to 50% occupancy with a *B*-factor of $\approx$27 Å^2.

In addition, a single strong peak of 8σ was observed in the F_o-F_c map, located at the dimer interface and was interpreted as a Pt ion. The interpretation was supported by calculation of an anomalous difference Fourier map that showed a significant peak at this position of 8.5σ. The site was refined with an occupancy of 0.2 and a *B*-factor of 30 Å^2. Attempts to set the Pt occupancy to higher or lower values led to either the F_o-F_c map showing extra negative or positive peaks or overly high or low *B*-factors for the Pt ion compared to surrounding side-chains. An additional

peak in the $2F_o-F_c$ map, attached to the Pt ion, was interpreted as a chloride ligand because of the high concentration of chloride in the crystallization medium. When modeled as an ammine group instead, a positive peak remained in the difference F_o-F_c map after refinement. The chloride ligand bound to the Pt center, refined to a *B*-factor of 25.3 Å^2 (with occupancy set to the same as the Pt ion). Trials to set the occupancy of the Pt–Cl complex to higher or lower values led to either the F_o-F_c map showing extra negative or positive peaks or the *B*-factors were too high or too low compared to surrounding side-chains. The Cys101 side-chains were modeled with two different conformations and had an average *B*-factor of 20 Å^2. The R_{cryst} for the final model is 17.6% (R_{free} of 21.5%) for all data to 1.85 Å resolution. A summary of the refinement statistics is given in Table 3. The model was analyzed with the program PROCHECK,[32] which showed that its stereochemical quality was similar or better than expected for structures refined at similar resolution.

An additional data set was collected at the Advanced Photon Source (Chicago, Illinois), on the GM/CA-CAT beam line 23ID-B by using a MARResearch MARmosaic 300 CCD detector tuned to 1.07 Å, the Pt L_3 edge, to maximize the anomalous signal from the Pt ion. This data set also resulted in a single large central peak at the dimer interface in the F_o-F_c map with a corresponding peak (6σ) in the anomalous difference map.

X-ray absorption spectroscopy and electrospray mass spectrometry of EA-CPT-GST P1-1 complexes in solution: The optimal conditions to achieve interaction of EA-CPT at the dimer interface of the protein were determined by sampling solutions with different ratios of protein to EA-CPT, both with and without GSH present. The concentration of complexes, following the dialysis and concentration steps, was approximately 0.75–1 mM prior to freezing. After purification the protein was stored in phosphate (10 mM, pH 7.0), EDTA (1 mM), and β-mercaptoethanol (1 mM). Post complex formation, DTT, and excess complex were dialysed away using the above buffer (but without β-mercaptoethanol). Reaction mixtures were analyzed by electrospray mass spectrometry on an Agilent 6510 Q-TOF LC/MS (Bio21 Institute, Melbourne University) with the following settings: fragmentor at 215 V, skimmer at 65 V and capillary voltage at 4000 V. Pt-GST P1-1 complexes were absent when equimolar or greater GSH was present in solution; instead the predominant species observed were low molecular weight Pt–glutathione complexes. Hence, GSH was excluded from solutions for further mass spectrometry measurements and the XAS experiments described below. Prior to all mass spectrometry and XAS experiments, the protein was incubated with excess DTT to ensure it was completely reduced and the solution was subsequently dialyzed to remove the DTT from solution which may effect EA-CPT binding. Thus DTT was added to a protein solution (30 mL of 2.5 mg mL^{-1}) to a final concentration of 10 mM. After 5 h, the solution was dialysed three times against buffer (5 L) for 4 h each to ensure the removal of all DTT. The protein was then incubated with compound for 10 h followed by a further three rounds of dialysis to remove excess compound for 4 h against buffer (5 L). The sample was then concentrated to 1 mg mL^{-1} and stored frozen.

Both size-exclusion chromatography and native gels indicated that, prior to the addition of EA-CPT, the protein existed exclusively as a dimer in solution in the concentration range studied (0.5–10 mg mL^{-1}). For the chromatography, Superdex 75 26/60 and Superdex 75 10/300 columns were used. The NativePAGE™ Novex® 4–16% Bis-Tris Gel system (Invitrogen) was employed for the native gels and the manufacturer's instructions were followed. Approximately 60% of GST P1-1 contained one additional N-terminal methionine, an artifact of the protein-expression procedure. Incubation of the protein with EA-CPT over several hours led to the formation of three distinct adducts. At incubation times up to 4 h, the only adduct observed had a *m*/*z* ratio consistent with the addition of one EA-CPT moiety to the protein dimer that included an extra Met residue. For incubation times longer than 4 h, two additional peaks were observed with *m*/*z* ratios corresponding to adducts of EA-CPT to either the dimer without the N-terminal methionine, or the dimer adduct formed at short incubation times. These data were interpreted to indicate that EA-CPT bound rapidly with the N-terminal methionine, where it was present, then reacted more slowly to form a second adduct with the dimer, presumably at the dimer interface.

The XAS sample was prepared by incubating EA-CPT (ca. 0.75 mM) with DTT-reduced protein (0.075 mM) for 6 h. The solution was subsequently dialyzed to remove excess EA-CPT and DMSO, followed by a tenfold concentration step to achieve a final complex concentration of approximately 0.75–1 mM. The complex was then frozen at −20 °C. Prior to data collection the sample was thawed and then flash-frozen in a 200 μL polycarbonate cuvette with a kapton window. XANES data were recorded at 10 K at the Australian National Beamline Facility (ANBF, beamline 20B at the Photon Factory, Tsukuba, Japan). L_3-edge Pt data were measured in fluorescence with a 35-pixel solid-state planar Ge detector (Eurisys). Harmonic rejection was achieved by detuning the channel-cut Si[111] monochromator by 50%. The energy scale was calibrated using a platinum foil as an internal standard (calibration energy, 11563.0 eV, corresponding to the first peak of the first derivative of the Pt L_3 edge). Background subtraction and normalization was achieved using BACKSUB software (G. N. George, unpublished).

Classical MD simulations of EA-CPT binding at the dimer interface: Five models, differing in the nature of the ligands directly coordinated to the Pt ion, were built using the crystal structure of the wild-type GST P1-1 complexed to EA-CPT as a reference. Each of these initial structures was immersed in a periodic box of approximately $87\times101\times95$ Å^3 containing about 21 500 water molecules, and neutralized with Na^+ counterions. The box dimensions were chosen to achieve a minimum distance of 30 Å between two periodically replicated images of the protein. The all-atom AMBER03 force field[33] was used to model standard protein residues and counterions, whereas the TIP3P model[34] was employed for water molecules. Van der Waals parameters for Pt ion were taken from previous studies,[35] whereas additional parameters for non-standard residues were derived from quantum chemical computations following the protocol described elsewhere.[36]

Electrostatic interactions were taken into account using the Particle Mesh Ewald algorithm[37] with a real space cutoff of 12 Å. The same cutoff was employed for the treatment of the van der Waals interactions. Bonds involving hydrogen atoms were constrained using the SHAKE algorithm.[38] An integration time step of 1 fs was used. Constant temperature (300 K) and pressure (1 atm) simulations were achieved by coupling the systems to a Langevin thermostat and a Nosé–Hoover Langevin barostat.[39,40] The systems were equilibrated using the following computational procedure: 1) structural optimization of solvent molecules using the conjugate gradient algorithm followed by 50 ps of MD; 2) energy minimization of the entire system (backbone protein atoms fixed) to remove bad contacts in the initial geometry; 3) heating of the system up to 300 K in 320 ps, while imposing positional restraints on the C_α atoms; 4) 6 ns of unrestrained constant temperature and pressure (NPT ensemble) in order to provide starting configurations for the subsequent QM/MM simulations. All the classical MD simulations were carried out using the NAMD package.[41]

QM/MM MD simulations of EA-CPT binding at the dimer interface: QM/MM MD simulations were performed starting from equilibrated configurations taken from the aforementioned classical runs. The quantum mechanical/molecular mechanical (QM/MM) implementation employed combines the use of the QM program QUICKSTEP[42] and the MM driver FIST, both part of the CP2K package (freely available at the URL http://cp2k.berlios.de, released under GPL license). In this code, the general QM/MM scheme is based on a real-space multigrid technique to compute the electrostatic coupling between both QM and MM regions.[43,44] In all the simulations, a quantum region consisting of the Pt center and the ligands directly coordinated to it, including both Cys101 side chains up to the C_β atom, was treated at the density functional theory (DFT) level, whereas the remaining part of the system, including water molecules and counterions, was modeled at the classical level using the AMBER force field to take explicitly into account the steric and electrostatic effects of the enzyme and solvent molecules. The valence of the terminal QM atoms was saturated by the addition of capping hydrogen atoms and a dual basis set, Gaussian and plane-wave (GPW) formalism, was employed to compute the interaction energy within the QM

subsystem. A triple-zeta valence basis set augmented with two sets of polarization functions (TZV2P) was used[45] to describe the wave function while an auxiliary plane-wave basis set expanded up to a density cutoff of 320 Ry was utilized to converge the electron density in conjunction with Goedecker–Teter–Hutter (GTH) pseudopotentials[46,47] to describe the core electrons. Exchange and correlation energies were computed within the generalized gradient approximation (GGA) by using the PBE functional.[48] All the ab initio MD simulations were performed within the Born-Oppenheimer approximation in the canonical (NVT) ensemble and using an integration time step of 0.5 fs. The QM region of each of the QM/MM structures was initially relaxed by performing a geometry optimization while the MM part was kept frozen. Then the systems were thermalized and further equilibrated for about 2 ps by using a Nosé–Hoover chain of thermostats[49] to maintain the temperature at 300 K. After equilibration each of the systems was run for 30 ps. Average values of structural parameters were computed from data collected over the last 15 ps of those trajectories.

Protein data bank accession numbers: The coordinates and structure factors have been deposited in the Protein Data Bank (http://www.rcsb.org/pdb/) under the filename 3N9J.

Acknowledgements

We thank Mike Gorman and Guido Hansen for advice and encouragement. We also thank the GM/CA staff for their help at the Advanced Photon Source. This work was supported by the Australian Synchrotron Research Program, which is funded by the Commonwealth of Australia under the Major National Research Facilities Program. Use of the Advanced Photon Source was supported by the U.S. DOE, Basic Energy Sciences, Office of Energy Research. This work was supported by grants from the Australian Research Council (ARC) to M.W.P. and H.H.H., the Australian Cancer Research Foundation to M.W.P. and from PRIN 2008 to M.L.B. P.C. thanks the Ministerio de Educación y Ciencia (MEC) and Fundación Española para la Ciencia y la Tecnología (FECYT) for financial support (ref. [2007]-0486). The CSCS (Manno, Switzerland) is acknowledged for providing access to its supercomputing facilities. Support from the Swiss National Science Foundation (Grant No. 200020-125173/1) is also gratefully acknowledged. L.J.P was supported by a National Health and Medical Research Council of Australia (NHMRC), Dora Lush Scholarship and an International Centre for Diffraction Data Crystallography Scholarship. D.B.A was an Australian Postgraduate Award Scholar and a recipient of a St. Vincent's Institute Foundation Scholarship sponsored by Colin North and Major Engineering. L.C.I. was supported by a St. Vincent's Institute Foundation award. H.H.H is an ARC Queen Elizabeth II Fellow and M.W.P. is an ARC Federation Fellow and NHMRC Honorary Fellow.

[1] A. Horwich, J. Shipley, R. Huddart, *Lancet* **2006**, *367*, 754–765.
[2] L. Kelland, *Nat. Rev. Cancer* **2007**, *7*, 573–584.
[3] M. A. Fuertes, C. Alonso, J. M. Perez, *Chem. Rev.* **2003**, *103*, 645–662.
[4] Y. W. Jung, S. J. Lippard, *Chem. Rev.* **2007**, *107*, 1387–1407.
[5] C. C. McIlwain, D. M. Townsend, K. D. Tew, *Oncogene* **2006**, *25*, 1639–1648.
[6] T. Nakajima, T. Takayama, K. Miyanishi, A. Nobuoka, T. Hayashi, T. Abe, J. Kato, K. Sakon, Y. Naniwa, H. Tanabe, Y. Niitsu, *J. Pharmacol. Exp. Ther.* **2003**, *306*, 861–869.
[7] D. Sheehan, G. Meade, V. M. Foley, C. A. Dowd, *Biochem. J.* **2001**, *360*, 1–16.
[8] J. D. Hayes, J. U. Flanagan, I. R. Jowsey, *Annu. Rev. Pharmacol. Toxicol.* **2005**, *45*, 51–88.
[9] M. C. Wilce, M. W. Parker, *Biochim. Biophys. Acta Protein Struct. Mol. Enzymol.* **1994**, *1205*, 1–18.
[10] G. Ferrandina, G. Scambia, G. Damia, G. Tagliabue, A. Fagotti, P. Benedetti Panici, C. Mangioni, S. Mancuso, M. D'Incalci, *Ann. Oncol.* **1997**, *8*, 343–350.
[11] S. Tsuchida, K. Sato, *Crit. Rev. Biochem. Mol. Biol.* **1992**, *27*, 337–384.
[12] C. R. Wolf, B. K. Park, N. Kitteringham, D. Otto, C. H. Henderson, *Chem.-Biol. Interact.* **2001**, *133*, 280–284
[13] S. Awasthi, S. K. Srivastava, F. Ahmad, H. Ahmad, G. A. Ansari, *Biochim. Biophys. Acta Protein Struct. Mol. Enzymol.* **1993**, *1164*, 173–178.
[14] J. H. Ploemen, B. van Ommen, P. J. van Bladeren, *Biochem. Pharmacol.* **1990**, *40*, 1631–1635.
[15] K. D. Tew, S. Dutta, M. Schultz, *Adv. Drug Delivery Rev.* **1997**, *26*, 91–104.
[16] W. H. Ang, I. Khalaila, C. S. Allardyce, L. Juillerat-Jeanneret, P. J. Dyson, *J. Am. Chem. Soc.* **2005**, *127*, 1382–1383.
[17] A. J. Oakley, J. Rossjohn, M. Lo Bello, A. M. Caccuri, G. Federici, M. W. Parker, *Biochemistry* **1997**, *36*, 576–585.
[18] M. D. Hall, G. J. Foran, M. Zhang, P. J. Beale, T. W. Hambley, *J. Am. Chem. Soc.* **2003**, *125*, 7524–7525.
[19] M. Iannuzzi, A. Laio, M. Parrinello, *Phys. Rev. Lett.* **2003**, *90*, 238302–238305.
[20] A. Laio, M. Parrinello, *Proc. Natl. Acad. Sci. USA* **2002**, *99*, 12562–12566.
[21] F. L. Gervasio, A. Laio, M. Parrinello, *J. Am. Chem. Soc.* **2005**, *127*, 2600–2607.
[22] M. Masetti, A. Cavalli, M. Recanatini, F. L. Gervasio, *J. Phys. Chem. B* **2009**, *113*, 4807–4816.
[23] W. H. Ang, Ph.D. Thesis, École Polytechnique Fédérale de Lausanne (Switzerland), **2007**.
[24] A. J. Oakley, M. Lo Bello, A. P. Mazzetti, G. Federici, M. W. Parker, *FEBS Lett.* **1997**, *419*, 32–36.
[25] A. Battistoni, A. P. Mazzetti, R. Petruzzelli, M. Muramatsu, G. Federici, G. Ricci, M. Lo Bello, *Protein Expression Purif.* **1995**, *6*, 579–587.
[26] L. J. Parker, S. Ciccone, L. C. Italiano, A. Primavera, A. J. Oakley, C. J. Morton, N. C. Hancock, M. Lo Bello, M. W. Parker, *J. Mol. Biol.* **2008**, *380*, 131–144.
[27] Joint CCP4 + ESF-EAMCB Newsletter on Protein Crystallography, A. G. W. Leslie, **1992**.
[28] Collaborative Computational Project, Number 4: *Acta Crystallogr. Sect. D* **1994**, *50*, 760–763.
[29] A. J. Oakley, M. Lo Bello, A. Battistoni, G. Ricci, J. Rossjohn, H. O. Villar, M. W. Parker, *J. Mol. Biol.* **1997**, *274*, 84–100.
[30] G. N. Murshudov, A. A. Vagin, E. J. Dodson, *Acta Crystallogr. Sect. A* **1997**, *53*, 240–255.
[31] P. Emsley, K. Cowtan, *Acta Crystallogr. Sect. A* **2004**, *60*, 2126–2132.
[32] R. A. Laskowski, M. W. MacArthur, D. S. Moss, J. M. Thornton, *J. Appl. Crystallogr.* **1993**, *26*, 283–291.
[33] Y. Duan, C. Wu, S. Chowdhury, M. C. Lee, G. Xiong, W. Zhang, R. Yang, P. Cieplak, R. Luo, T. Lee, *J. Comput. Chem.* **2003**, *24*, 1999–2012.
[34] W. L. Jorgensen, J. Chandrasekhar, J. D. Madura, R. W. Impey, M. L. Klein, *J. Comput. Phys.* **1983**, *79*, 926–935.
[35] S. Yao, J. P. Plastaras, L. G. Marzilli, *Inorg. Chem.* **1994**, *33*, 6061–6077.
[36] W. D. Cornell, P. Cieplak, C. I. Bayly, I. R. Gould, K. M. Merz, D. M. Ferguson, D. C. Spellmeyer, F. T. , J. W. Caldwell, P. A. Kollman, *J. Am. Chem. Soc.* **1993**, *115*, 5179–5197.
[37] U. Essmann, L. Perera, M. L. Berkowitz, T. Darden, H. Lee, L. G. Pedersen, *J. Chem. Phys.* **1995**, *103*, 8577–8593.
[38] J. P. Ryckaert, G. Ciccotti, H. J. C. Berendsen, *J. Comput. Phys.* **1977**, *23*, 327–341.
[39] S. E. Feller, Y. Zhang, R. W. Pastor, B. R. Brooks, *J. Chem. Phys.* **1995**, *103*, 4613–4621.
[40] G. Martyna, D. Tobias, M. Klein, *J. Chem. Phys.* **1994**, *101*, 4177–4189.
[41] L. Kalé, R. Skeel, M. Bhandarkar, R. Brunner, A. Gursoy, N. Krawetz, J. Phillips, A. Shinozaki, K. Varadarajan, K. Schulten, *J. Comput. Phys.* **1999**, *151*, 283–312.
[42] J. VandeVondele, M. Krack, F. Mohamed, M. Parrinello, T. Chassaing, J. Hutter, *Comput. Phys. Commun.* **2005**, *167*, 103–128.

[43] T. Laino, F. Mohamed, A. Laio, M. Parrinello, *J. Chem. Theory Comput.* **2005**, *1*, 1176–1184.
[44] A. Laio, J. VandeVondele, U. Rothlisberger, *J. Chem. Phys.* **2002**, *116*, 6941–6948.
[45] A. Schaefer, C. Huber, R. Ahlrichs, *J. Chem. Phys.* **1994**, *100*, 5829–5835.
[46] S. Goedecker, M. Teter, J. Hutter, *Phys. Rev. B* **1996**, *54*, 1703–1710.
[47] C. Hartwigsen, S. Goedecker, J. Hutter, *Phys. Rev. B* **1998**, *58*, 3641–3662.
[48] J. P. Perdew, K. Burke, M. Ernzerhof, *Phys. Rev. Lett.* **1996**, *77*, 3865–3868.
[49] S. Nosé, *J. Chem. Phys.* **1984**, *81*, 511–519.

Received: February 22, 2011
Published online: June 16, 2011

